Role of the Edge and Scrape-Off Layer Plasma in Lower Hybrid Current Drive Experiment on Alcator C-Mod

S. G. Baek[1, a)], B. Biswas[1], P. T. Bonoli[1], D. Brunner[1,2], I. C. Faust[1,3], A. E. Hubbard[1], J. W. Hughes[1], B. LaBombard[1], R. T. Mumgaard[1,2], M. Porkolab[1], S. Shiraiwa[1], G. M. Wallace[1], S. J. Wukitch[1]

[1]*MIT Plasma Science and Fusion Center, Cambridge, MA USA 02139*
[2]*Present affiliation: Commonwealth Fusion Systems, Cambridge, MA USA 02139*
[3]*Present affiliation: Max Planck Institute for Plasma Physics, Garching, Germany 85748*
[a)] *Corresponding author: sgbaek@psfc.mit.edu*

Abstract. This paper reports the latest lower hybrid current drive (LHCD) experimental and modeling investigations conducted on Alcator C-Mod, which further elucidates the role of the scrape-off layer (SOL) in determining the magnitude and profile of wave power deposition. In the latest C-Mod LHCD experiment, with a proper management of the SOL plasma, a recovery of efficient current drive is observed in a diverted configuration at densities exceeding the previously identified LH density limit of $\bar{n}_e \approx 1.0\text{x}10^{20}$ m^{-3}. By operating at higher current, i.e., at lower Greenwald fraction, the SOL width is reduced and the turbulence level is minimized. Under this condition, parasitic wave power losses occurring in the edge/SOL region are found to be minimized. In our modeling study, a shift or spread in the poloidal mode number by the SOL turbulence is investigated in order to better match the experimental power deposition profile with an available ray-tracing/Fokker-Planck model. The approach is to introduce an additional spectral broadening mechanism by launching the rays with a non-negligible poloidal wavenumber component while preserving the launched $n_{//}$ power spectrum. This approach contrasts to spectral broadening achieved in the $n_{//}$ space. An initial modeling investigation on the C-Mod plasma reproduces an experimental on-axis power deposition profile.

Introduction

Radio frequency (RF) heating and current drive is expected to play a crucial role in solving the sustainment challenge in a fusion tokamak reactor. While the core wave physics is well understood, the interaction of the RF wave with the edge/SOL plasma is recently gaining attention due to possible deleterious impacts to RF wave propagation and absorption. In a tokamak reactor, the RF waves launched from the antenna at the tokamak vessel must cross the turbulent edge/SOL plasma. In addition to the presence of incoherent fluctuations, density perturbations that have a coherent spatial structure in the plane perpendicular to the magnetic field have been characterized in the tokamak boundary region. Such density perturbations known as the blobs are identified to be responsible for determining the SOL density profile by convecting out the plasma particles and by increasing wall recycling [1]. More importantly, this blobby transport is experimentally found to scale with the Greenwald fraction. Therefore, the interaction of RF waves with the edge/SOL plasma needs be characterized in order to project the performance of the RF actuator to that in a reactor condition, which will operate near or above the Greenwald density limit.

Recent experiments show that lower hybrid current drive (LHCD) faces two challenges arising from the presence of the cold and dense SOL. One is to understand and overcome the "LH density limit" problem [2]—an anomalous loss of current drive efficiency at high densities. This limit behavior has been observed since the beginning of LHCD experiments [see, for example, 3]. The C-Mod study [4] has identified that a divertor configuration worsens the problem compared to the limiter configuration [5,6]. The second challenge is to properly model the impact of density fluctuations on wave propagation. Since density fluctuations are always present at the tokamak boundary region, a

proper treatment of the interaction between LH waves and density fluctuations may provide insights into the widely observed discrepancy of wave damping profile between the experiment and model. Specifically, wave power is observed to damp on-axis in the present-day experiment that operates in a multi-pass damping regime, while the model predicts an off-axis power deposition [7–9].

This paper reports the latest experimental and modeling investigations conducted on Alcator C-Mod, which further elucidates the role of the edge/SOL plasma in determining wave propagation and absorption behaviors. C-Mod officially completed its operation in 2016, and the experimental data taken are under active analysis. Efficient LHCD is demonstrated for the first time in a diverted configuration at high density by operating at a low Greenwald fraction. In our modeling investigation using GENRAY/CQL3D [10,11] in πScope [12], spectral broadening in the perpendicular wave-vector space is investigated, which will be shown to provide a mechanism of on-axis power deposition without a need to modify the antenna $n_{//}$ power spectrum.

Loss of LHCD Efficiency at High Density in a Divertor Configuration

The LHCD experiment on Alcator C-Mod is designed such that ω_0/ω_{LH} $(\bar{n}_e, B_0)$ remains above 2 in order to stay above the LH density limit previously established based on the onset of parametric decay instabilities (PDIs) [13]. Here, ω_0 is the applied LH frequency, and $\omega_{LH}(\bar{n}_e, B_0)$ is the lower hybrid frequency $(= \omega_{pi}/\sqrt{1 + \omega_{pe}^2/\omega_{ce}^2})$ evaluated using the line-averaged density, $\bar{n}_e$ and the central magnetic field, B_0. However, the C-Mod experiment in a divertor configuration exhibited a loss of LHCD efficiency initiated at low densities when $\omega_0/\omega_{LH} < 4$, or equivalently when $\bar{n}_e > 1.0\text{x}10^{20}$ m^{-3} [2]. In those experiments, the plasma current was set to a typical C-Mod operating plasma current at 0.8 MA. Under this plasma condition, as shown in Fig. 1, the hard X-ray diagnostic measurement indicates an exponentially decaying population of the fast electrons. This scaling is in contrast to the synthetic diagnostic result that predicted a weak inverse scaling to density (blue line in Fig. 1). Experimentally, the injected wave power is found to be either radiated or conducted to the divertor in a time scale much faster than the energy confinement time scale [14], indicating that the injected wave power is promptly lost at the plasma edge without being absorbed in the plasma core.

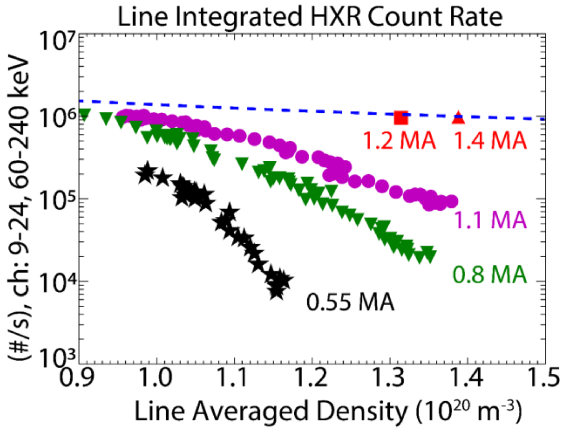

FIGURE 1. Line integrated hard X-ray count rates versus the line-averaged density at five different plasma currents.

Several parasitic wave-edge/SOL interactions that can be responsible for the loss of efficiency have been identified on C-Mod. Two multi-pass loss mechanisms have been investigated. First, collisional power loss is found to be significant on C-Mod as the waves propagate across the edge/SOL plasma multiple times before being absorbed in the plasma [2]. Up to 90% of the injected power is found to be lost via collisions particularly near the X-point region with a realistic 2-D SOL model [8]. Another multi-pass loss mechanism identified is a strong $n_{//}$ up-shift predicted by a full wave code when the wave-fields reflect off the inner-wall side [15]. The LHCD efficiency is inversely proportional to $n_{//}^2$. First-pass loss mechanisms are also characterized. Ion cyclotron PDIs have been detected with RF probes installed at the plasma boundary [16–18]. They were found to be initiated in front of the launcher at a high density. Furthermore, the decrease in the measured pump peak power correlated with the saturation of the PDI sideband power, implying that PDIs can contribute to the observed loss of efficiency. The growth rate calculation

shows a maximum growth rate near the LCFS, in line with the experimental identification of the rf power damping location around the LCFS. At the same time, pump broadening is also observed, an indication of wave scattering by edge turbulence. It can alter the wave spectral component and limit the radial wave penetration [19].

SOL Profile Control with Plasma Current

As noted earlier, the C-Mod experiments [1] have identified that the SOL density profile is a function of the Greenwald fraction, $f_G \equiv \bar{n}_e/n_G$, where $n_G \equiv I_p/(\pi a^2)$ is the Greenwald density limit. Figure 2 shows that, by raising I_p, the width of the SOL density reduces without a formation of the "shoulder" structure (i.e., the flat density profile in the 0.55 MA case). This is due to the reduced cross-field particle flux at a low Greenwald fraction, as shown Fig. 2(b). A low level of the SOL density helps mitigate collisional power loss and the PDI onset. A low level of plasma density fluctuation also mitigates wave scattering. Therefore, the impact of the edge/SOL plasma on LHCD can be weakened by operating at a low f_G, which can be achieved by raising I_p for the given line-averaged density.

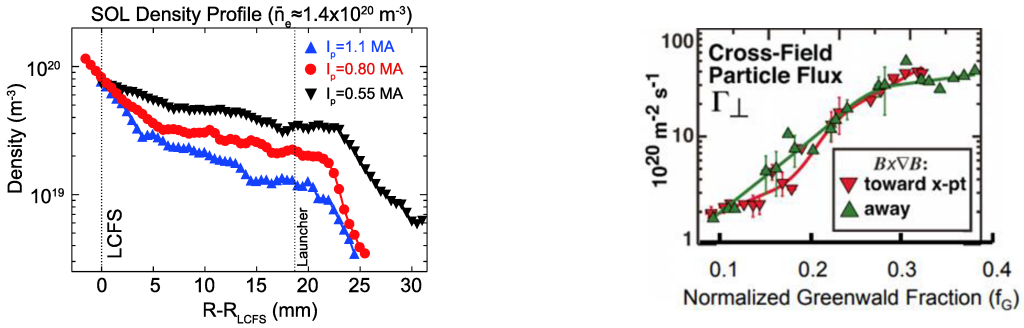

(a) (b)

FIGURE 2. (a) SOL density profile measured at three different plasma currents, while maintaining the same line-averaged density. Figure is reproduced from Fig. 13 of [17]; (b) Cross-field particle flux in the SOL induced by the density fluctuation as a function of the Greenwald fraction. Figure reproduced from Fig. 4 of [1].

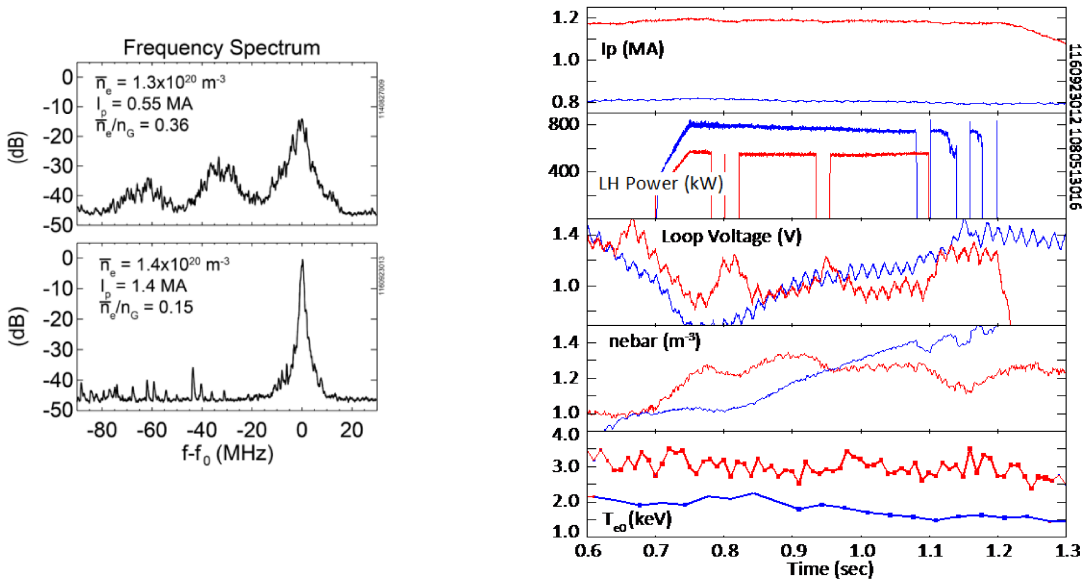

(a) (b)

FIGURE 3. (a) LH frequency spectra measured at two different Greenwald fractions at the fixed line-averaged density. f_0 = 4.6 GHz. A detailed study of the PDI onset as a function of density at different currents is presented in [17]. (b) Time traces of two plasma discharges at 1.2 MA (red) and 0.8 MA (blue).

Recovery of LHCD Efficiency at High Density

C-Mod experiments in the 2016 experimental campaign [20] investigated the LH density limit problem by lowering the Greenwald fraction to below 20% by raising the plasma current up to I_p = 1.4 MA with B_{t0} = 7.8 T. Raising the magnetic field helps maintain a similar q-profile to the 0.8 MA and 5.4 T operation. Under this low Greenwald fraction, the rf probe measurement indicates that parasitic wave losses are largely suppressed up to near the core wave accessibility of $\bar{n}_e \approx 1.5\text{x}10^{20}$ m^{-3}. As shown in Fig. 3(a), the PDI sidebands are absent in the 40 dB range below the pump peak power with a minimized pump broadening. Figure 3(b) compares the two plasma discharges at I_p =1.2 MA in red and 0.8 MA in black as a reference case. At a high current, effective LHCD is evidenced by the drop in loop voltage with an injection of LH power. A detailed analysis presented in [20] shows that this change in loop voltage is consistent with the LHCD efficiency observed at a low density [21]. In the high current case (1.2 MA), the central temperature $T_{e0} \approx 3$ keV remains nearly constant, indicating that the drop of loop voltage is due to RF current drive. Furthermore, a substantial increase in the HXR rates is also observed, as shown in Fig. 1. Note that the total count rates follow the expected density scaling that is inversely proportional to the line-averaged density at the two high currents (1.2 and 1.4 MA) [10,11]. It is worth pointing out that the observed increase in the HXR counts is not attributed to the presence of the background electric field. While the loop-voltage (≈ 1 V) remains high in these plasmas due to the limited amount of wave power, a similar level of the background ohmic field is also present in the low current plasma that exhibited the LH density limit behavior (e.g., see the third panel in Fig. 3(b)). Therefore, it is concluded that the observed recovery of the expected scaling in the HXR production rates is due to the suppression of edge loss mechanisms at high I_p, evidenced by the spectral measurement shown in Fig 3(a). While not shown here, the standard GENRAY/CQL3D can reproduce the observed experimental level of ~10^6 #/s shown in Fig. 1 within a factor of three [20], implying that parasitic losses are suppressed in the low Greenwald fraction plasma. This is the first demonstration of effective LHCD at high densities over the LH density limit in a diverted configuration, and provides a path forward to implementing LHCD at a reactor-level density. An implication of this work is discussed at the end of the paper.

Impact of Edge/SOL Fluctuations on Wave Propagation at Low Density

In this section, we focus in the low density regime where efficient current drive is observed but the experimental current drive profile does not match to the modeled profile. This has motivated us to examine how the edge/SOL density fluctuations can modify wave propagation and absorption in the low density regime. As shown in Fig. 2, density fluctuations, while at a varying degree, are always present at the tokamak boundary. While efficient lower hybrid current drive is observed in this low density regime, the challenge remains to understand the experimental power deposition profile that robustly exhibits on-axis power damping despite a large variation in the plasma condition or the wave parameter such as the injected $n_{//}$ power spectrum [22]. Standard ray-tracing/Fokker-Planck models, which rely on a geometrical $n_{//}$-upshift for wave damping, tend to predict off-axis power deposition due to a strong $n_{//}$ up-shift when the rays propagate toward the plasma center after reflecting off the cut-off layer at the plasma boundary. It is a well-known effect [23] arising from the geometrical evolution of the poloidal mode number in a toroidal geometry, which prevents wave power from being deposited in the plasma core in the multi-pass damping regime. In order to resolve the discrepancy between the experiment and modeling, previous studies introduced a spectral broadening in the $n_{//}$ space [7,24]; by re-distributing the initial antenna power spectrum to the high $n_{//}$ components, on-axis power deposition is reproduced. In this case, the synthetic HXR profile reconstructed from the model is also in good agreement with the experimental result that exhibits a bell-shaped profile with a broad maximum around the central chord of the HXR diagnostic that intersects the plasma center [22].

In our work, spectral broadening in the perpendicular wave-vector ($\vec{k}_\perp$) space is introduced. This is a phenomenological model in order to identify under which condition the experimental profile is reproduced with a modeling. In a typical ray-tracing model, a single ray represents a single $n_{//}$ component of the antenna power spectrum. To simulate the wave spectral component imposed by the antenna structure, the perpendicular wave-vector of the ray is directed along the radial ($\nabla\psi$) direction, so that χ, the angle between $\vec{k}_\perp$ and $\nabla\psi$, is zero at the initial position of the ray. However, when the wave propagates through the turbulent SOL region, wave scattering by the density fluctuations induced by drift-wave turbulence [19,23] is known to scatter the directionality of the wave $\vec{k}_\perp$. The three wave interaction occurs mainly via a coupling of the perpendicular wave-vectors. In the parallel direction, the fluctuation wave-vector has a much longer parallel wavelength than that of the LH wave-vector, hence the parallel wave-vector

($\vec{k}_\parallel$) of the LH wave remains largely unaffected. While the previous theoretical work does not take into account blobs that have a spatially coherent structure, we expect a similar effect in the presence of the blobs. A recent measurement on C-Mod indicates the presence of a finite poloidal component of the LH electric field vector in front of the launcher [25]. Depending on the amount of angular rotation that a wave experiences, the spectral components of k_φ and k_θ can be written in terms of χ as the following [10]:

$$k_\varphi = k_\perp \sin\chi \frac{B_\theta}{B} + k_\parallel \frac{B_\varphi}{B} \quad (1)$$

$$k_\theta = -k_\perp \sin\chi \frac{B_\varphi}{B} + k_\parallel \frac{B_\theta}{B} \quad (2)$$

Note that both $\vec{k}_\perp$ and $\vec{k}_\parallel$ conserve their magnitudes before and after wave scattering [23] . Equation (2) also shows that, the initial k_θ is a small quantity under a typical condition of $\chi \approx 0$ because $\sin\chi \approx 0$ and $\frac{B_\theta}{B} \ll 1$. With an angular rotation, however, $\vec{k}_\perp$ now possesses the finite toroidal and poloidal components as the following:

$$\vec{k}_\perp = k_\perp \sin\chi \left(\hat{e}_\varphi \frac{B_\theta}{B} - \hat{e}_\theta \frac{B_\varphi}{B}\right) + k_\perp \cos\chi\, \hat{e}_\psi \quad (3)$$

Figure 4(a) shows the variation of the components of the refractive-index vector as a function of χ. $\vec{k}_\perp$ is purely radial at $\chi = 0$. In the present study, the angular space of interest is limited to be: $|\chi| < \frac{\pi}{2}$ in order to ensure that the group velocity is in the direction toward the plasma center, i.e., $k_\perp \cos\chi > 0$ in Eq. (3). Note that, with $\chi > 0$, $\vec{k}_\perp$ has a poloidal component parallel to $\vec{B}_\theta$ in the C-Mod configuration. On the other hand, when $\chi < 0$, $\vec{k}_\perp$ has a poloidal component anti-parallel to $\vec{B}_\theta$. Figure 4(b) shows a set of the unit vectors of $\vec{k}_\perp$ in the R and Z plane. Note that the toroidal term inside the parenthesis in Eq. (3) does not contribute much to $\vec{k}_\perp$ since $\frac{B_\theta}{B} \ll 1$. Therefore, in determining the angular orientation of $\vec{k}_\perp$, the radial term dominates over the poloidal term when χ is small, and vice versa when χ is large.

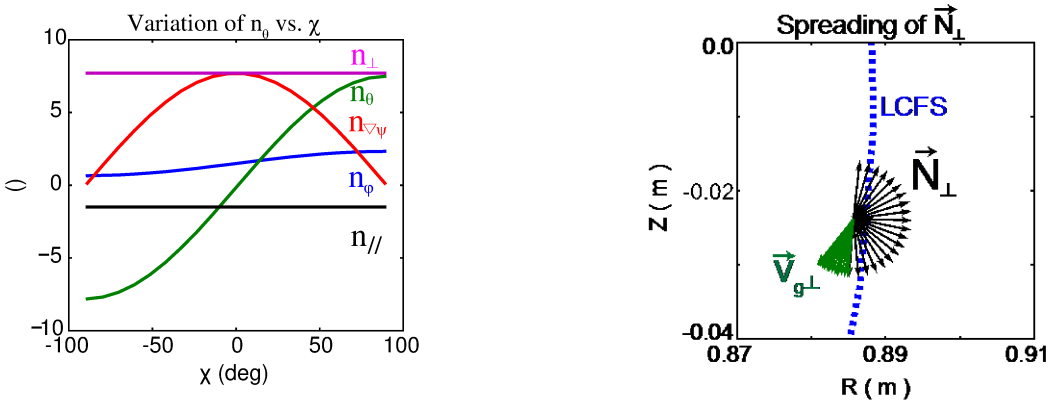

(a) (b)

FIGURE 4. (a) Variation of the refractive index vector components as a function of the angle χ between $\vec{k}_\perp$ and $\nabla\psi$. (b) Unit vectors of the perpendicular refractive index vector (in black) as a function of χ, and the corresponding group velocity vectors (in green) projected in the R-Z plane.

Figure 4(a) also shows that the scattering process does not alter the magnitude of the parallel wave-vector ($|\vec{k}_\parallel|$). However, the composition of $\vec{k}_\parallel$ varies as a function χ as the following [23]:

$$k_\parallel = \vec{k} \cdot \vec{B}/|\vec{B}| \approx k_\varphi + \frac{k_\theta r}{R_0} \frac{1}{q(r)} \quad (4)$$

where k_φ and k_θ are defined in Eqs. (1) and (2), and $q(r)$ is the safety factor. Therefore, the scattering process provides a mechanism for generating a finite initial k_θ component that can readily contribute to the ray evolution

through the variation of both $q(r)$ and the poloidal mode number ($m \equiv k_\theta r$) in a toroidal geometry that exhibits a poloidal dependence of $\frac{dm}{d\theta} \approx -k_\parallel R_0 q(r) \frac{r}{R_0} \sin\theta$ [23]. It shows that the m variation is maximized when the ray is located at $|\theta| \rightarrow \pi/2$. In the present-day multi-pass damping regime, this k_θ term is initially a small term under an assumption of $\chi \approx 0$, and the ray needs one or two bounces before this term becomes significant enough to contribute to the $\vec{k}_\parallel$ evolution.

Figure 5 compares the three different pairs of ray trajectories with different degrees of angular rotation. In all cases, the initial $n_\parallel$ = -1.63 remains the same. In the C-Mod geometry, with the negative angular rotation, the rays exhibit a direct radial penetration to the plasma center and deposit its power on the first pass. On the other hand, with the positive angular rotation, the poloidal term in Eq. (4) has an opposite sign to that of the toroidal term, which prohibits the first-pass $k_\parallel$ up-shift. However, the ray experiences the up-shift on the second pass at the high-field-side boundary. Therefore, the effect of negative $\vec{k}_\perp$-rotation is to enhance the first-pass absorption to the plasma core and to reduce the ray sensitivity to the plasma condition with a reduced the ray propagation path, while positive rotation leads to weaker penetration and absorption in the core.

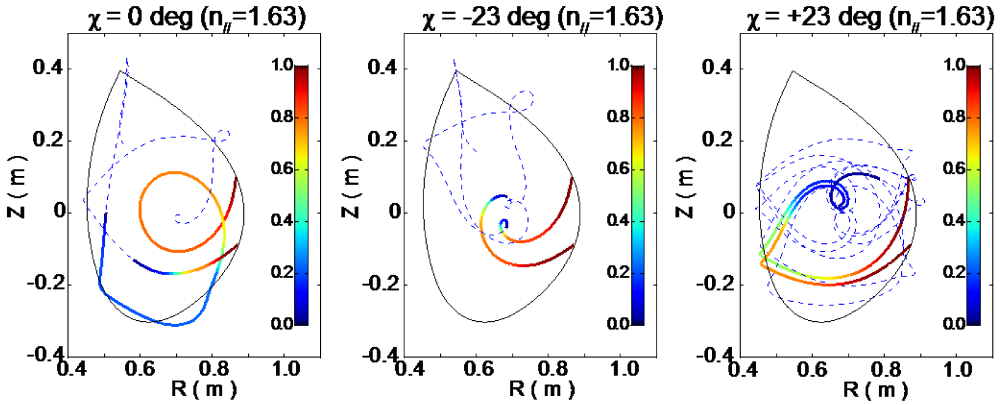

(a) (b) (c)

FIGURE 5. Ray trajectories with (a) χ = 0, (b) χ = -23 deg, and (c) χ = +23 deg. The rays all have the same the initial $n_\parallel$ = -1.63. The color-bar denotes the normalized ray power to the initial ray power. The two rays are launched at the LCFS near the outboard midplane. The beginning of the dotted lines corresponds to when the ray power becomes 1% of the initial ray power.

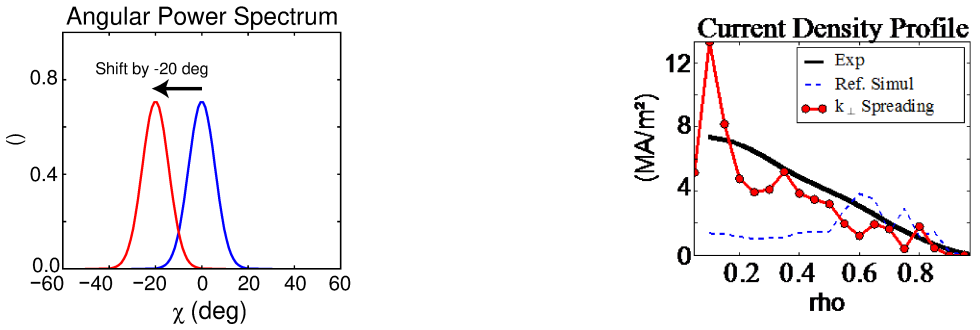

(a) (b)

FIGURE 6. (a) Two Gaussian power spectrum assumed as a function of χ. (b) Comparison of the experimental current density profile and the modeled profiles with a shifted power spectrum (in red) and the reference simulation without $\vec{k}_\perp$-rotation (in blue). The experimental total plasma current is 530 kA.

Figure 6(a) shows an example of two power spectra assumed in our study. To simulate the scattering effect, a ray that represents the single $n_{//}$ power component is decomposed into a set of multiple rays that follow the Gaussian power spectrum in the angular space. This assumption is in line with the previous work by Andrews and Perkins [19], who

showed that the angular power spectrum converges to the cosine distribution centered at χ=0 in the limit of strong wave scattering. Another power spectrum broadened in χ and shifted to the negative angular side is also investigated in order to enforce the first-pass penetration. Under this condition, the current profile modeled matches well to the experimental profile, as shown in Fig. 6(b). Without this spectral broadening, the model predicts an off-axis power deposition profile. In order to understand the implication of the spectral shift shown Fig 6(a), a more detailed comparison against the experimental result will be presented in a separate publication.

Implication of LHCD Experiment at a High Density

Figure 7 shows the LHCD operation regime of the present-day devices as a function of the Greenwald fraction (f_G) and the ratio of the source frequency to the lower hybrid frequency evaluated using the line-averaged density $\omega_0/\omega_{LH}(\bar{n}_e)$. Here, $\omega_0/\omega_{LH}(\bar{n}_e)\rightarrow 2$ is a rule of thumb criterion for the PDI limit, while f_G is a proxy for the level of SOL turbulence. The color bar denotes the line-averaged density. As discussed earlier, the C-Mod experiment demonstrates that the PDI onset can be avoided by operating at a low Greenwald fraction (< 20%) achieved by raising the plasma current. It is worth repeating that a lower f_G leads to a lower SOL density due to the decreased level of particle transport, which increases the convective PDI threshold. It also minimizes collisional power loss and wave scattering, correlated with the improved LHCD performance. EAST [26,27] avoids the PDI onset by raising $\omega_0/\omega_{LH}(\bar{n}_e)$ with an use of the 4.6 GHz wave. Nevertheless, PDIs might not be a sole mechanism that determines the LH density limit behavior. The experiments on Tore Supra [28] and FTU [29]report the same LH density limit behavior in their high density regime without the PDI onset, which is consistent with the observation that $\omega_0/\omega_{LH}(\bar{n}_e)$ remains above 4. It should be noted that both tokamaks operate with a limiter configuration. On the other hand, Tore Supra and FTU operate at a high Greenwald fraction (> 0.5) under which a turbulent SOL is expected compared to C-Mod and EAST. As the tokamak reactor will operate near or above the Greenwald limit in order to maximize the fusion gain, the impact of wave scattering on wave propagation needs to be evaluated at a high Greenwald fraction. In particular, the SOL plasma of the H-mode plasma needs to be investigated in detail.

The placement of the launcher on the high field side [30] can be beneficial to suppress the first-pass loss mechanisms studied in this paper. The measurement on C-Mod shows that the SOL at the high-field-side of the tokamak has a steep density gradient and a negligible level of turbulence with a double null operation [31]. In this regard, the proposed LHCD experiment of high-field-side launch at DIII-D led by MIT [32] could be an important test-bed to investigate a role of first-pass loss mechanisms on the LH density limit problem because the waves are expected to be absorbed in the plasma core on the first-pass, while interacting with the edge/SOL plasma only once in front of the launcher.

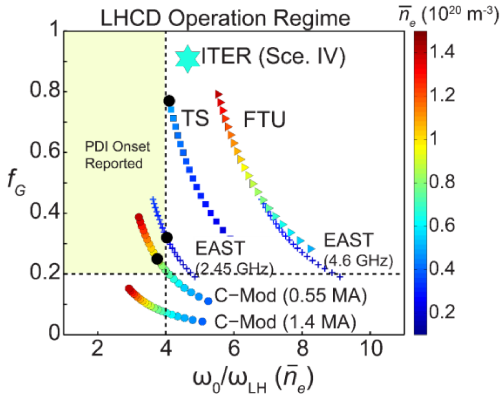

FIGURE 7. Lower hybrid current drive operation regime as a function of the Greenwald fraction (f_G) and the ratio of the source frequency to the lower hybrid frequency evaluated using the line-averaged density ($\omega_0/\omega_{LH}(\bar{n}_e)$). The color bar denotes the line-averaged density.

ACKNOWLEDGEMENTS

This research was conducted on Alcator C-Mod, which is a DOE Office of Science User Facility, and supported by US Department of Energy: DE-FC02-99ER54512 and DESC0010492.

REFERENCES

[1] B. Labombard, J. W. Hughes, N. Smick, A. Graf, K. Marr, R. McDermott, M. Reinke, M. Greenwald, B. Lipschultz, and J. L. Terry, Phys. Plasmas **15**, 056106 (2008).

[2] G. M. Wallace, R. R. Parker, P. T. Bonoli, A. E. Hubbard, J. W. Hughes, B. L. LaBombard, O. Meneghini, A. E. Schmidt, S. Shiraiwa, D. G. Whyte, and others, Phys. Plasmas **17**, 082508 (2010).

[3] W. Hooke, Plasma Phys. Control. Fusion **26**, 133 (1984).

[4] G. M. Wallace, A. E. Hubbard, P. T. Bonoli, I. C. Faust, R. W. Harvey, J. W. Hughes, B. L. LaBombard, O. Meneghini, R. R. Parker, A. E. Schmidt, and others, Nucl. Fusion **51**, 083032 (2011).

[5] Y. Takase, M. Porkolab, J. J. Schuss, R. L. Watterson, C. L. Fiore, R. E. Slusher, and C. M. Surko, Phys. Fluids **28**, 983 (1985).

[6] M. Porkolab, J. J. Schuss, B. Lloyd, Y. Takase, S. Texter, P. Bonoli, C. Fiore, R. Gandy, D. Gwinn, B. Lipschultz, and others, Phys. Rev. Lett. **53**, 450 (1984).

[7] Y. Peysson, J. Decker, E. Nilsson, J. F. Artaud, A. Ekedahl, M. Goniche, J. Hillairet, B. Ding, M. Li, P. T. Bonoli, and others, Plasma Phys. Control. Fusion **58**, 044008 (2016).

[8] S. Shiraiwa, S. G. Baek, I. Faust, G. Wallace, P. Bonoli, O. Meneghini, R. Mumgaard, R. Parker, S. Scott, R. W. Harvey, and others, in *AIP Conf. Proc.* (AIP Publishing, 2015), p. 030016.

[9] C. Yang, P. T. Bonoli, S. Shiraiwa, B. Ding, M. H. Li, S. Frank, and X. Zhai, Phys. Plasmas **25**, 082516 (2018).

[10] A. Smirnov, R. Harvey, and K. Kupfer, Bull Amer Phys Soc **39**, 1626 (1994).

[11] R. W. Harvey and M. C. McCoy, in *Proc IAEA Tech. Comm. Meet. Adv. Simul. Model. Thermonucl. Plasmas* (IAEA, Vienna (1993), 1992), p. 527.

[12] S. Shiraiwa, T. Fredian, J. Hillairet, and J. Stillerman, Fusion Eng. Des. **112**, 835 (2016).

[13] M. Porkolab, Phys. Fluids **20**, 2058 (1977).

[14] I. C. Faust, D. Brunner, B. LaBombard, R. R. Parker, J. L. Terry, D. G. Whyte, S. G. Baek, E. Edlund, A. E. Hubbard, J. W. Hughes, and others, Phys. Plasmas **23**, 056115 (2016).

[15] O. Meneghini, C. Lau, S. Shiraiwa, G. M. Wallace, R. R. Parker, B. L. LaBombard, I. C. Faust, J. R. Wilson, and S. J. Wukitch, in *AIP Conf. Proc.* (AIP, 2011), pp. 411–418.

[16] S. G. Baek, R. R. Parker, S. Shiraiwa, G. M. Wallace, P. T. Bonoli, D. Brunner, I. C. Faust, A. E. Hubbard, B. LaBombard, and M. Porkolab, Plasma Phys. Control. Fusion **55**, 052001 (2013).

[17] S. G. Baek, R. R. Parker, P. T. Bonoli, S. Shiraiwa, G. M. Wallace, B. LaBombard, I. C. Faust, M. Porkolab, and D.G. Whyte, Nucl. Fusion **55**, 043009 (2015).

[18] S. G. Baek, R. R. Parker, S. Shiraiwa, G. M. Wallace, P. T. Bonoli, M. Porkolab, Y. Takase, D. Brunner, I. C. Faust, A. E. Hubbard, and others, Phys. Plasmas **21**, 061511 (2014).

[19] P. L. Andrews and F. W. Perkins, Phys. Fluids **26**, 2546 (1983).

[20] S. G. Baek, G. M. Wallace, P. T. Bonoli, D. Brunner, I. C. Faust, A. E. Hubbard, J. W. Hughes, B. LaBombard, R. R. Parker, and M. Porkolab, Phys. Rev. Lett. **121**, 055001 (2018).

[21] P. T. Bonoli, J. Ko, R. Parker, A. E. Schmidt, G. Wallace, J. C. Wright, C. L. Fiore, A. E. Hubbard, J. Irby, E. Marmar, and others, Phys. Plasmas **15**, 056117 (2008).

[22] R. T. Mumgaard, Lower Hybrid Current Drive on Alcator C-Mod: Measurements with an Upgraded MSE Diagnostic and Comparisons to Simulation, PhD Thesis, Massachusetts Institute of Technology, 2015.

[23] P. T. Bonoli and E. Ott, Phys. Fluids **25**, 359 (1982).

[24] J. Decker, Y. Peysson, J.-F. Artaud, E. Nilsson, A. Ekedahl, M. Goniche, J. Hillairet, and D. Mazon, Phys. Plasmas **21**, 092504 (2014).

[25] E. H. Martin, C. Lau, G. M. Wallace, S. Shiraiwa, and R. T. Mumgaard, Nucl. Fusion **59**, 076006 (2019).

[26] B. J. Ding, E. H. Kong, M. H. Li, L. Zhang, W. Wei, M. Wang, H. D. Xu, Y. C. Li, B. L. Ling, Q. Zang, and others, Nucl. Fusion **53**, 113027 (2013).

[27] M. H. Li, B. J. Ding, F. K. Liu, J. F. Shan, M. Wang, H. D. Xu, L. Liu, H. C. Hu, X. J. Zhang, Y. C. Li, and others, Phys. Plasmas **23**, 102512 (2016).

[28] M. Goniche, V. Basiuk, J. Decker, P. K. Sharma, G. Antar, G. Berger-By, F. Clairet, L. Delpech, A. Ekedahl, J. Gunn, and others, Nucl. Fusion **53**, 033010 (2013).

[29] R. Cesario, L. Amicucci, A. Cardinali, C. Castaldo, M. Marinucci, L. Panaccione, F. Santini, O. Tudisco, M. L. Apicella, G. Calabrò, and others, Nat. Commun. **1**, 55 (2010).

[30] P. T. Bonoli, G. M. Wallace, S. Shiraiwa, S. G. Baek, J. Doody, M. Greenwald, B. LaBombard, R. Leccacorvi, K. Filar, and Y. Lin, Nucl. Fusion **58**, 126032 (2018).

[31] N. Smick, B. LaBombard, and C. S. Pitcher, J. Nucl. Mater. **337**, 281 (2005).

[32] S. J. Wukitch, S. Shiraiwa, G. M. Wallace, P. T. Bonoli, C. Holcomb, and R. I. Pinsker, in *EPJ Web Conf.* (EDP Sciences, 2017), p. 02012.